Loss measurement of plasmonic modes in planar metal–insulator–metal waveguides by an attenuated total reflection method

Chien-I Lin and Thomas K. Gaylord*

School of Electrical and Computer Engineering, Georgia Institute of Technology, Atlanta, Georgia 30332-0250, USA
**Corresponding author: tgaylord@ece.gatech.edu*

Received August 16, 2010; revised October 15, 2010; accepted October 20, 2010;
posted October 21, 2010 (Doc. ID 132775); published November 9, 2010

We report experimental excitation and characterization of surface plasmon modes in planar metal–insulator–metal (MIM) waveguides. Our approach is based on determining the width of the reflection angular spectrum in the attenuated total reflection (ATR) configuration. Owing to its transverse character, the ATR configuration provides a more straightforward and simpler way to determine the loss of plasmonic modes in MIM structures, compared to using tapered end couplers with multiple waveguide samples or scanning near-field optical microscopy. In this Letter, two waveguide structures with Au claddings and 50/200 nm SiO_2 cores are investigated. The propagation lengths measured at $\lambda = 1.55$ μm are 5.7 and 18 μm, respectively, in agreement with the theoretical predictions.

OCIS codes: 240.6680, 230.7370, 250.5300.

Surface plasmon (SP)-based waveguides have been considered as promising candidates in realizing integrated optical nanocircuitry, owing to their subwavelength confinement and their "slow-wave" nature [1–4]. Among the family of various SP-based waveguides, metal–insulator–metal (MIM) waveguides have the best lateral confinement because of the relatively shallow field penetration (approximately a skin depth) into the metal claddings. However, the loss in MIM waveguides is substantial, owing to the intrinsic loss of the metal, and it is further magnified by the narrow transverse modal confinement [3,4], which, in turn, is essential in integration of SP-based nanocircuitry. Therefore, the simulation and measurement of the loss in MIM waveguides are critically important in the development of SP-based optical nanocircuitry. However, the aperture and the modal profile of a typical MIM structure are usually below the diffraction limit [3,4]. Therefore, the excitation of a MIM plasmonic mode typically requires end-fire coupling with tapered fibers or waveguides. Further, the loss can be measured by using multiple waveguide structures with various length scales [5,6], in which the coupling strength may vary from sample to sample and is difficult to quantify, or scanning near-field optical microscopy (SNOM) [7–9], which is sensitive to noncontrollable environmental factors, such as vibration and temperature.

The approach presented here is based on the concept of the transverse transmission/reflection (TTR) method [10,11], which significantly simplifies the loss measurement of the MIM plasmonic modes. The TTR method differs from previous loss measurement methods for MIM waveguides [5–9]. Instead of injecting light through the end of a waveguide [5–7], the TTR method excites a plasmonic mode from the transverse direction. This can be realized by making one of the metal claddings sufficiently thin (e.g., three to four skin depths) for light coupling [9,11]. A high-index prism is then added adjacent to the thin metal layer to enable coupling (see Fig. 1). By measuring the reflectance as a function of the wave vector of the incident wave, the Lorentzian minima are located at the real parts of the propagation constants, and the half-width at half-minima (HWHM) of these resonances are equal to the imaginary parts of the propagation constants of the allowed plasmonic modes. Therefore, the TTR method provides a straightforward and simple approach for determining the complex propagation constants by using a configuration similar to the prism coupler introduced by Ulrich and Tien [12,13] and to the attenuated total reflection (ATR) configuration [14–16]. However, to date, to the best of our knowledge, no such experiments have been applied to characterize the plasmonic modes in a MIM structure.

The prism-loaded MIM structure in Fig. 1 can be analyzed by using the transfer matrix formulation. According to [11], the reflectance R can be expressed as

$$R \simeq R_{\mathrm{SP}}\left[1 - S(\beta)\cdot\frac{\alpha_{\mathrm{MIM}}}{(\beta-\beta_{\mathrm{MIM}})^2+\alpha_{\mathrm{MIM}}^2}\right], \qquad (1)$$

where β is the z component of the incident wave vector, $S(\beta)$ is a slowly varying function of β, and β_{MIM} and α_{MIM} are the phase and attenuation propagation constants of the MIM plasmonic mode, respectively. R_{SP} is equal to R as $d_m \to \infty$, which is usually referred to as the Otto

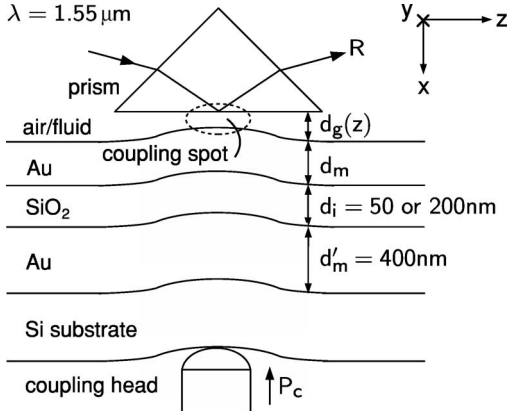

Fig. 1. Schematic diagram of the ATR configuration applied to the MIM structures.

configuration [17]. Equation (1) shows that R is similar to R_{SP}, but the former has one or more resonances corresponding to the MIM plasmonic modes near $\beta = \beta_{MIM}$. In this Letter, only the symmetric TM_0 mode is of interest. Equation (1) also indicates that R/R_{SP} has a Lorentzian-type resonance centered at $N_{MIM} \equiv \beta_{MIM}/k_0$ and a HWHM $= \alpha_{MIM}/k_0$. It is shown in [11] that R/R_{SP} can be obtained by simply subtracting out the background variation (i.e., R_{SP}) from R.

The schematic diagram of the experimental configuration is shown in Fig. 1. The measurements were performed by using a Metricon Model 2010 prism coupler [18], which uses a coupling head to push the waveguide structure toward the prism to create a coupling spot. The force is controlled by the pressure, P_c, which is adjustable from 10 to 50 psi, or equivalently, from 69 to 345 kPa. A laser beam can be manually adjusted to be centered on the coupling spot for a stronger coupling between the prism and the MIM plasmonic mode. MIM structures with two different SiO_2 core thicknesses, $d_i = 50$ and 200 nm, were fabricated and characterized at $\lambda = 1.55$ μm. The Au layer on the top of the structure should be 75 to 100 nm in thickness, which is about three to four skin depths, to ensure appropriate coupling strength. The Au layer substrate is 400 nm in thickness, which, for practical purpose, is optically semi-infinite. The Au cladding layers were deposited by using an e-beam evaporator at a rate of 0.05 nm/s, and the SiO_2 cores were deposited by using plasma-enhanced chemical vapor deposition at 250 °C, 900 m Torr, with 400 SCCM SiH_4 (2% in N_2), 900 SCCM N_2O, and rf power = 10 W (SCCM denotes cubic centimeters per minute at standard temperature and pressure).

The theoretical propagation constant of the MIM structure can be rigorously calculated by using the argument principle method [19]. At $\lambda = 1.55$ μm, the refractive index of Au is $n_{Au} = 0.53 - j10.79$ [20], and the refractive index of SiO_2 is $n_{SiO_2} = 1.49$. The relatively high index of SiO_2 might be a result of incomplete oxidization at low rf power [21,22]. The calculated normalized propagation constants are $(\beta_{MIM} - j\alpha_{MIM})/k_0 = 1.6574 - j0.0082$ and $2.073 - j0.0259$ for the 200 and 50 nm cores, respectively.

Figure 2 illustrates the reflection power spectra measured at various fluid ($n_g = 1.4459$) gap thicknesses d_g for the structure in Fig. 1 with $d_m = 60$ nm and $d_i = 200$ nm. The relatively smaller d_m is used for a stronger TM_0 resonance and therefore a greater contrast to the resonance of the fluid gap–metal mode. In this case, the gap thickness d_g is changed by moving the laser beam from the center of the coupling spot (d_{g1}) to off-center locations (d_{g2}, d_{g3}). For d_{g1}, the gap is small (<100 nm) and the coupling between the prism and the TM_0 mode of the MIM structure is the strongest. The fluid gap thicknesses can be estimated by comparing the measured reflection spectra with the simulated ones, which are based on the transfer matrix [10,11]. For d_{g3}, the gap is the largest (~1 μm) and the coupling to the TM_0 mode is negligible. The structure is practically an Otto configuration [11,17], and a prominent SP mode in the fluid gap–metal interface is observed, with an effective index very close to the index of the fluid $n_g = 1.4459$. At the intermediate gap thickness d_{g2}, both the resonances of the fluid gap–metal SP mode and the

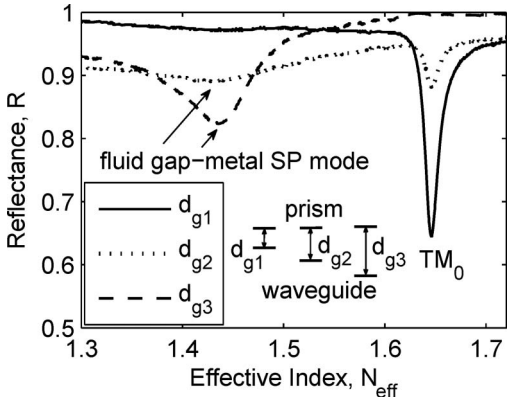

Fig. 2. Reflection power spectra measured at various fluid ($n_g = 1.4459$) gap thickness d_g values. The x axis is the effective index of the incident beam, $N_{eff} \equiv \beta/k_0$. The resonances corresponding to the fluid gap–metal SP mode and the TM_0 mode of the MIM structure are labeled.

TM_0 mode can be observed. Therefore, to characterize the TM_0 mode, the laser beam is adjusted to be centered on the coupling spot for a stronger resonance. In the following two cases with differing oxide thicknesses, the laser beam is aligned in this manner.

The reflection power spectra for the structure in Fig. 1 with $d_m = 80$ nm and $d_i = 200$ nm is shown in Fig. 3(a). By increasing the pressure of the coupling head, P_c, the air gap thickness d_g decreases and a series of spectra were measured. The resonances of R correspond to the TM_0 mode of the MIM structure, which are centered at $N_{MIM} = 1.6560$ in this case. Figure 3(b) shows the normalized attenuation coefficients $\alpha_{MIM}/k_0 =$ HWHM versus P_c. There is no apparent trend in α_{MIM}/k_0 as a function of P_c. This implies that there is no requirement on P_c (and, therefore, d_g), provided the TM_0 resonance is adequately observable. This also indicates that the slightly nonplanar coupling spot has little effect on the measurement results. The HWHM are obtained after removing the background variation in R_{SP}; this can be done by leveling both sides of a resonance to unity. The average of the measurements yields $\alpha_{MIM}/k_0 = 0.0070$, with a standard deviation = 0.0001. This is equivalent to a

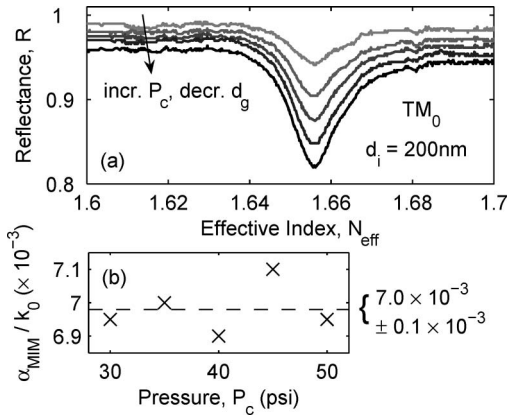

Fig. 3. (a) Reflection power spectra for the structure in Fig. 1 with $d_m = 80$ nm and $d_i = 200$ nm measured at various air gap thicknesses d_g, which correspond to pressures of the coupling head, $P_c = 30, 35, 40, 45$, and 50 psi. (b) Normalized attenuation coefficients $\alpha_{MIM}/k_0 =$ HWHM for the resonance at various values of P_c.

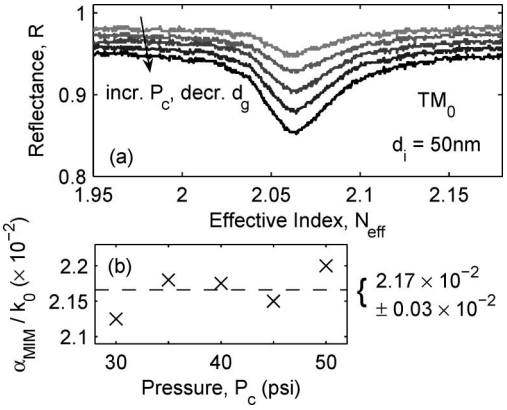

Fig. 4. (a) Reflection power spectra for the structure in Fig. 1 with $d_m = 80$ nm and $d_i = 50$ nm measured at various air gap thicknesses d_g corresponding to $P_c = 30$, 35, 40, 45, and 50 psi. (b) Normalized attenuation coefficients $\alpha_{\mathrm{MIM}}/k_0 = \mathrm{HWHM}$ for the resonance at various values of P_c.

loss of 0.25 dB/μm or 18 μm in propagation length. The experimental results agree well with the theoretical calculations. The ~15% smaller measured loss may be due to the better film quality, as observed by [6].

Figure 4(a) shows the reflection power spectra for the structure in Fig. 1 with $d_m = 80$ nm and $d_i = 50$ nm at various air gap thicknesses d_g. The TM_0 resonances are centered at $N_{\mathrm{MIM}} = 2.0635$ in this case. Figure 4(b) shows $\alpha_{\mathrm{MIM}}/k_0 = \mathrm{HWHM}$ versus P_c. Again there is no apparent trend in $\alpha_{\mathrm{MIM}}/k_0$ as a function of P_c. The average of the measurements yields $\alpha_{\mathrm{MIM}}/k_0 = 0.0217$, with a standard deviation = 0.0003. This is equivalent to a loss of 0.76 dB/μm or 5.7 μm in propagation length. The experimental results agree well with the theoretical calculations.

To summarize, the loss in plasmonic modes in MIM structures are measured based on the TTR method. Because of its transverse nature, the ATR configuration obviates the need for tapered end couplers and multiple waveguide samples or SNOM. Moreover, the TTR method may be extended to characterize higher-order modes in MIM structures; this is nearly infeasible for the end-coupling type of loss measurements. The TTR method is therefore a powerful tool for characterizing MIM structures, and it could facilitate the typically complicated and challenging development of SP-based optical nanocircuitry.

References

1. H. Raether, *Surface Plasmons on Smooth and Rough Surfaces and on Gratings* (Springer-Verlag, 1988).
2. W. L. Barnes, A. Dereux, and T. W. Ebbesen, Nature **424**, 824 (2003).
3. E. Ozbay, Science **311**, 189 (2006).
4. E. Feigenbaum and M. Orenstein, J. Lightwave Technol. **25**, 2547 (2007).
5. T. Goto, Y. Katagiri, H. Fukuda, H. Shinojima, Y. Nakano, I. Kobayashi, and Y. Mitsuoka, Appl. Phys. Lett. **84**, 852 (2004).
6. J. A. Dionne, H. J. Lezec, and H. A. Atwater, Nano Lett. **6**, 1928 (2006).
7. S. I. Bozhevolnyi, V. S. Volkov, E. Devaux, and T. W. Ebbesen, Phys. Rev. Lett. **95**, 046802 (2005).
8. J. C. Weeber, Y. Lacroute, and A. Dereux, Phys. Rev. B **68**, 115401 (2003).
9. E. Verhagen, J. A. Dionne, L. Kuipers, H. A. Atwater, and A. Polman, Nano Lett. **8**, 2925 (2008).
10. C.-I. Lin and T. K. Gaylord, Appl. Opt. **48**, 3603 (2009).
11. C.-I. Lin and T. K. Gaylord, Appl. Opt. **49**, 936 (2010).
12. R. Ulrich, J. Opt. Soc. Am. **60**, 1337 (1970).
13. P. K. Tien and R. Ulrich, J. Opt. Soc. Am. **60**, 1325 (1970).
14. A. E. Craig, G. A. Olson, and D. Sarid, Opt. Lett. **8**, 380 (1983).
15. J. C. Quail, J. G. Rako, and H. J. Simon, Opt. Lett. **8**, 377 (1983).
16. F. Z. Yang, G. W. Bradberry, and J. R. Sambles, Phys. Rev. Lett. **66**, 2030 (1991).
17. A. Otto, Z. Phys. **216**, 398 (1968).
18. Metricon Corporation, http://www.metricon.com/.
19. E. Anemogiannis and E. N. Glytsis, J. Lightwave Technol. **10**, 1344 (1992).
20. P. B. Johnson and R. W. Christy, Phys. Rev. B **6**, 4370 (1972).
21. A. C. Adams, F. B. Alexander, C. D. Capio, and T. E. Smith, J. Electrochem. Soc. **128**, 1545 (1981).
22. S. Matsuo and M. Kiuchi, Jpn. J. Appl. Phys. **22**, L210 (1983).